Optics Letters

Direction-resolved homodyne laser-Doppler vibrometry by analyzing space-time fringes created by the successive 1D intensity profiles of the interference fringes

Mohammad Hossein Daemi[1] and Saifollah Rasouli[1,2,*]

[1]Department of Physics, Institute for Advanced Studies in Basic Sciences, Zanjan 45137-66731, Iran
[2]Optics Research Center, Institute for Advanced Studies in Basic Sciences, Zanjan 45137-66731, Iran
*Corresponding author: rasouli@iasbs.ac.ir

Received 29 August 2019; accepted 30 September 2019; posted 4 October 2019 (Doc. ID 375558); published 27 November 2019

In this Letter, we introduce a simple direction-resolved homodyne Laser-Doppler vibrometry method by sewing successive one-dimensional images of the interference pattern recorded by a linear array detector and creating a two-dimensional space-time fringe pattern. A space-time fringe pattern visualizes the vibration form, and it can be used for characterizing the vibration of the object. We measure the vibration of a harmonically driven loudspeaker as a known source to demonstrate the capability of the method. We also employ the method to characterize the vibrational properties of the resonator elements of a thin-disk laser. The method reveals the environmental and instrumental sources of the vibration. The use of an array detector in the detection system simplifies the fringe chasing procedure and optical setup and, by the aid of a space-time image, the vibration waveform is directly determined with no requirement for a time-consuming SPS algorithm.

https://doi.org/10.1364/OL.44.005824

Vibration is a very important phenomenon in a vast area of science and technology. It can also have a predominant effect on the intensity and phase noises of the laser beams, which can affect their applications [1]. Therefore, measurement of the vibration parameters can help to improve different types of laser products. Thin-disk lasers (TDLs) are attracting great attention by providing high-power and high-quality beams in CW and pulsed modes [2]. Due to the mentioned advantages, TDLs found diverse applications in science and technology [3]. The performance of the resonator components of the laser is affected by the vibration. The vibration measurement of the resonator should be non-contact and sometimes remote. Laser-Doppler vibrometry (LDV) fully satisfies both of these conditions [4,5]. Usually a point detector records the intensity fluctuation in the observation plane of a two-beam interferometer. The intensity fluctuation is the consequence of the out-of-plane vibration that is experienced by a mirror of the interferometer. However, there are some deficiencies here. Except for very small amplitudes of the vibration ($A < \lambda/4$, λ is the wavelength of the probe beam) and in a special tuning of the interferometer's equilibrium arms named *quadrature point*, the detected signal does not discriminate against the motion direction of the mirror. To prevent the instrument from drifts due to environmental conditions, some efforts were made to maintain the interferometer in the quadrature point [6], which can complicate the instrument. Heterodyne LDV [7] is one of the well-established methods that can bypass the problem. In this method, a high-frequency shift (some tens of megahertz, usually using an acousto-optic cell) is implemented on the reference beam. Then there will be a high-frequency beating in the detection plane, even in the absence of the vibration. The motion of the vibrating mirror alters the beating frequency, and the alteration sign reveals the direction of the motion. Other alternative methods, which are referred to as pseudo-heterodyne methods, have also been used to create the large frequency shift [8,9]. Another smart method is known as the quadrature detection [10,11]. In this method, two linearly polarized components of a circularly polarized reference beam having a $\pi/2$ relative phase lag interfere with two similar copies of the linearly polarized measure beam. Since the resulting interfering signals have a $\pi/2$ relative phase shift, by the ratio of the DC-subtracted parts of these signals, the vibration form, including the direction information, can be reconstructed. We have recently used a fringe chasing method by three-point spatial phase shifting (SPS) for discrimination of motion direction in the long-range homodyne LDV [12]. Here we use another method for chasing the fringes using a linear array sensor that demonstrates the motion details very intuitively, without the need for an SPS procedure.

After a short description of the equations governing homodyne LDV, we will explain the used method. After that, we will show the results of measurements on a loudspeaker with a known frequency of vibration in order to describe the method and its ease of use. Then we will show the results of vibrometry of the gain medium of a TDL. The gain medium is a thin disk

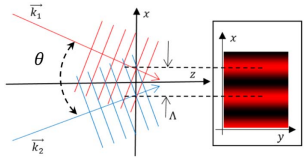

Fig. 1. Interference of two mutually coherent beams having a tilt angle relative to each other leads to a straight-line fringe pattern. Any frequency shift for one of the beams causes the pattern to move with a velocity proportional to the value of the frequency shift.

of Yb:YAG crystal that is bounded on the surface of a substrate in which its back side impinged with the cooling water jet [13].

The intensity response function of a typical Michelson interferometer to the out-of-plane displacement of one of its mirrors is a harmonic function of the out-of-plane displacement Z_m:

$$I(t) = a + b\cos(2kZ_m(t)), \tag{1}$$

in which $k = 2\pi/\lambda$ is the wavenumber of the probe laser, illuminating the interferometer. The parameters a and b are the DC level and modulation of the intensity signal, respectively. This modulation of the intensity is the beating between two coherent beams. When the displacement is an accelerated motion, the signal has a chirped nature. By tilting one of the mirrors and producing an angle θ between two interfering beams, one can produce parallel straight-line fringes (see Fig. 1).

We can rewrite the intensity distribution as

$$I(x,t) = a(x) + b(x)\cos\left(\frac{2\pi}{\Lambda}x + \Phi(t)\right), \Lambda = \frac{\lambda}{2\sin(\theta/2)}, \tag{2}$$

where Λ is the inter-fringe distance and, $\Phi(t)$ is the phase of the fringe pattern at the origin $x = 0$. The x-direction is considered to be perpendicular to the fringe lines. Parameters a and b are time independent. The time dependence of the phase Φ of the cosine function in Eq. (2) is due to the motion of the mirror, which leads to the motion of the fringe pattern. One can easily prove that the displacement of the fringe pattern x_F depends on the displacement of the mirror via the following simple linear relation [12]:

$$Z_m(t) = x_F\sin\left(\frac{\theta}{2}\right) = \frac{\lambda}{2}\times\frac{x_F}{\Lambda}. \tag{3}$$

According to this equation, if we chase a specific fringe of the pattern during the experiment, we can reconstruct the mirror's motion. In the experiment, a nearly straight-line fringe pattern is formed on a one-dimensional (1D) array detector in which the direction of fringes is almost perpendicular to the direction of the array. The images in Fig. 2 are produced using a Michelson interferometer. To detect the signal, we use a linear sensor array, TSL1402, with 256 pixels and a maximum sampling rate of $f_s \le 19157$ Hz. The pitch of the pixels is 63.5 μm, and the total length is about 16.25 mm. We align the fringe direction to be nearly perpendicular to the sensor array direction. We create a two-dimensional (2D) *space-time* image (STI) by sewing successive 1D images of the array detector. At the first sight, this image yields the overall waveform of the interference fringe motion during the vibration. Figure 2(a) demonstrates an example of such a STI for LDV of a 20 Hz

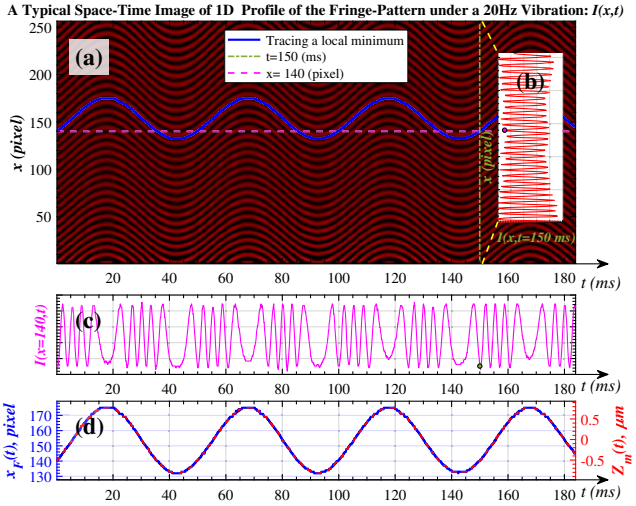

Fig. 2. (a) Typical STI of the fringe profile recorded in the LDV of a loudspeaker, which is driven harmonically with a frequency of 20 Hz. The data acquisition rate is $f_s = 9785$ line/s, where a 180 ms time interval of the STI is shown. The probe beam wavelength is 633 nm from a He–Ne laser. The fringe period is calculated through a Fourier method as 8.53 pixel equivalent to 0.56 mm with $\theta = 1.13$ mrad. (b) 1D profile of the fringe pattern at time $t = 150$ ms. (c) Intensity signal experienced by the pixel No. 140 of the array sensor in the time interval of (a). (d) Reconstructed motion of the fringe, $x_F(t)$, using a fringe-tracing algorithm (left vertical axis) and the calculated motion of the object $Z_m(t)$ (right vertical axis) in the same time interval. The vibration amplitude is about 0.8 μm. The limits of the vertical axes are adjusted in order for the waveforms to overlap (see Visualization 1).

vibration of a loudspeaker diaphragm. Figures 2(b) and 2(c) show the corresponding 1D intensity profile along the x-direction and recorded intensity signal by a given pixel, respectively. The temporal evolution of the peaks and valleys is evident in the image. Each bright or dark line in this image imitates the interference fringes motion (see Visualization 1). Figure 2(d) shows the trace of a given local minimum fringe of the STI that demonstrates the motion form of the object. To extract the temporal behavior of a given minimum on the 1D fringe profile, we follow the subsequent simple algorithm:

- At the first column of the STI (the first sample), select an arbitrary peak (or valley) around the middle region of the column and assign it as the position of the fringe at the beginning of the vibration $x_f(t = 0)$.
- Find the location of the nearest peak (or valley) in the next adjacent column as the fringe position at the $x_f(t = \delta t)$. Here $\delta t = 1/f_s$ is the sampling time interval.
- Repeat this procedure n times to acquire the temporal behavior of the interferometric fringe pattern in the $[0\ n\delta t)$ time span.
- In the cases where x_f is near the upper or lower edge of the image, change the calculation point to around the middle point again, but consider adding the amount of this jump $(x_{f,\mathrm{New}} - x_{f,\mathrm{Old}})$ to the subsequent calculated data. The jump is similar to the phase wraps in the interferometry.

After doing this procedure, the fringe temporal evolution is obtained. Employing Eq. (3), the motion of interferometer's

mirror $Z_m(t)$ can be reconstructed. In order to use this equation, we need the parameter Λ. One can calculate Λ by averaging the peak distance in a column of the image or by doing discrete Fourier transform on the dataset of that column. Figure 3(a) shows the interferometer setup for LDV measurements on a loudspeaker. HR1, HR2, and HR3 are high-reflection flat mirrors. FSL is a spherical lens for focusing the measure beam on the target. This focusing is necessary for the elimination of the effect of the curvature of the vibrating object. ISL is a spherical lens for imaging the beam on the array sensor. This lens with focal length of 4 cm located at 20 cm from the sensor is also used to magnify the interference area in order to have a suitable size on the sensor. Figure 3(b) shows the necessary modification to the optical setup to do measurements on the gain medium of a TDL located in the resonator enclosure. As the laser output coupler mirror, OC, is installed at the normal angle to the disk, the measure beam passed inclined into the resonator enclosure [through windows Win1 and Win2, see Fig. 3(b)], and the beam impinges the disk with an incident angle of about 60 mrad. We considered the effect of inclined incidence in the optical path calculations. A flat mirror HR4 redirects the measure beam back to the disk and then toward the interferometer. Because the used disk has a dioptric power of about 0.3 m^{-1}, over its cross section, the measure beam is not an ideal spherical wave. Due to the curvature of the thin disk and inclined incidence of the beam on it, the reflected beam experiences an astigmatism over the entire wavefront. Interfering this beam with a plane wave will not produce straight lines in the observation plane. To overcome this difficulty, we add a spherical lens SL3 to the measure beam prior to HR4 mirror. The focal plane of this lens is approximately on the HR4. Tuning the position of the lens alongside the beam will adjust the measure beam wavefront at the beam splitter to be nearly flat. Because the distance from the observation windows to the disk is about 1 m, the optical path difference between two arms is in the order of 2 m. This difference was tuned to be an integer multiple of the cavity length of the probe He–Ne laser (37 cm) in order to fully employ the coherent repeat length of a laser source. In the calculations, the effect of a double path survey of the beam is considered.

Figure 4 shows a piece of STI of the LDV measurement on the disk, in the presence of environmental intense noise of the fans. In Fig. 5, the reconstructed motion and its spectrum are depicted for this experiment. As is clear from the spectrum, a high amplitude around 21.5 Hz vibration is dominant. The small peaks at 100 Hz may be attributed to the fake signal

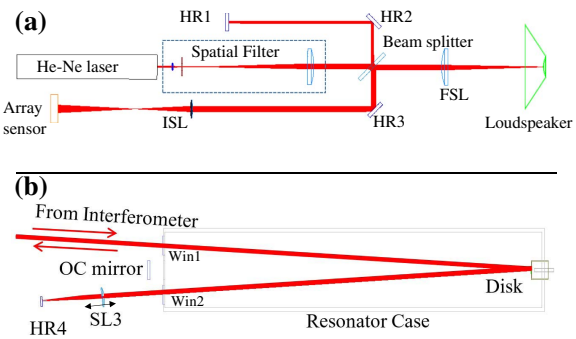

Fig. 3. (a) Michelson interferometer setup for LDV of a loudspeaker. (b) Optical setup for LDV of the gain medium of a TDL.

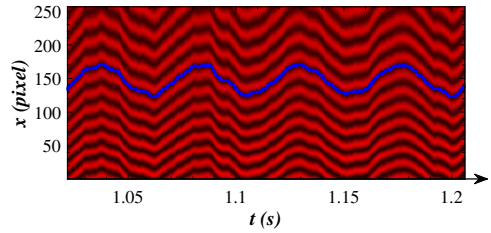

Fig. 4. Piece of the STI of the LDV measurement on the disk in the presence of environmental intense noise of the fans (see Visualization 2). The fringe period is a 23.3 pixels, equivalent to 1.48 mm with $\theta = 0.43$ mrad.

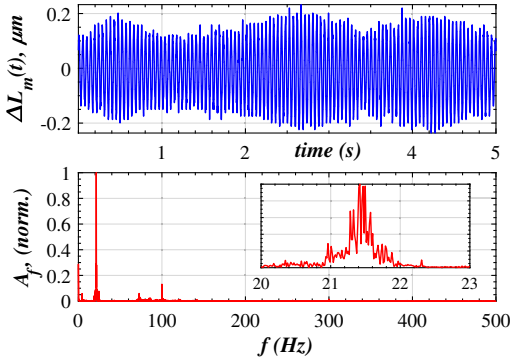

Fig. 5. Reconstructed vibration waveform of Fig. 4 and its spectrum. For clarity of demonstration, the waveform is shown in a 5 s period.

of fluorescent lamps. (Visualization 2 demonstrates the use of the proposed algorithm for reconstruction of this non-harmonic vibration.)

Figure 6 shows the corresponding STI for the impulse response of the mechanical structure of the disk module, assembled outside the resonator enclosure, where it permits us to impinge the measure beam perpendicularly to the disk. For this measurement, the speaker in Fig. 3(a) is replaced with the disk module. Because of the changes in the mounting system, the vibration characters may differ from the case in which the disk was mounted inside the resonator enclosure. Figure 7 shows the reconstructed motion and its spectrum for the impulse response. Having more than one predominant peaks in the spectrum indicates that the structure is a kind of multiple degree of freedom system.

To determine the applicable limits of the method, we consider a harmonic motion and introduce the *amplitude-period*

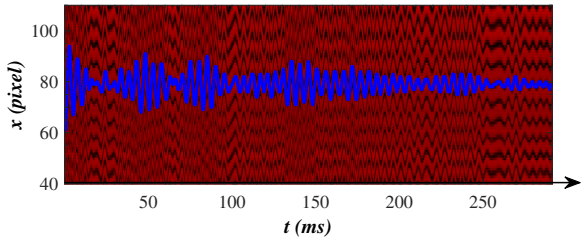

Fig. 6. STI of impulse response of a disk mount outside the resonator enclosure.

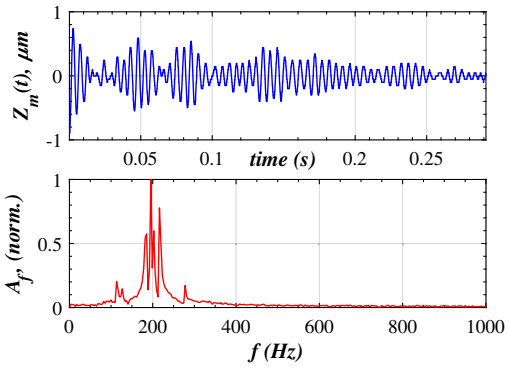

Fig. 7. Reconstructed motion and its spectrum for the impulse response related to Fig. 6.

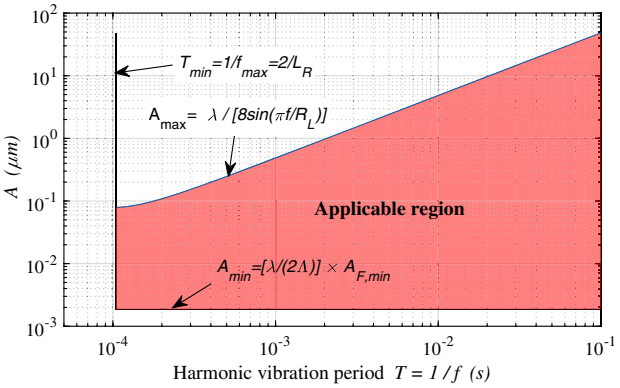

Fig. 8. Applicable region of the method on the amplitude-period plane. The semi-transparent red region is where the method can reconstruct the motion form.

plane (Fig. 8). Each point with coordinates (T, A) defines a harmonic vibration with amplitude A and frequency $f = 1/T$.

In a vibration with a small amplitude (typically $A < \lambda/4$), the signal calculated from Eq. (1) imitates the waveform of the vibration. Based on the Nyquist's criterion the maximum detectable frequency is $R_L/2$, with R_L as the line rate of the array detector. Therefore, in the amplitude-period plane, the applicable region for the STI method is left-bounded by the line $T_{\min} = 1/f_{\max} = 2/R_L$. For higher values of the vibration amplitude, the intensity signal at each pixel of the detector exhibits a different waveform, which is a chirped waveform [see Fig. 2(c) with $A = 1.26\lambda$]. In this case, to avoid aliasing, the maximum measurable displacement of the fringe pattern in a time interval between two recorded successive line frames should be less than one-half of the fringe spatial period. This means that, at the same time interval, the maximum measurable displacement of the object is $\Delta x_{\max} = \lambda/4$. For a sinusoidal wave, in a time interval equal to the acquisition period $1/R_L$, the uppermost displacement occurs for the quadrature point and is given by

$$\Delta x = x\left(t = \frac{1}{2R_L}\right) - x\left(t = \frac{-1}{2R_L}\right) = 2A \sin\left(\frac{\pi f}{R_L}\right), \quad (4)$$

and the maximum measurable vibration amplitude of the object is given by

$$A_{\max} = \lambda/8 \sin(\pi f/R_L). \quad (5)$$

This region is also lower-bounded by the minimum measurable amplitude $A_{\min} = (\lambda/2) \times (A_{F,\min}/\Lambda)$, imposed by the minimum detectable fringe vibration amplitude $A_{F,\min}$ and Λ values. We consider $A_{F,\min} = 1$, but one can optimize it to a sub-pixel region by a suitable fitting of a curve to the intensity profile at nearby pixels [14]. By increasing Λ, one can measure smaller displacements. In order for the proposed algorithm be applicable at the jumps, we limit the maximum Λ to $2N/3$ with N as the total number of pixels (1.5 period in the sensor span). By considering $N = 256$, we estimated the minimum measurable displacement as 2 nm. In Fig. 8, by considering the specifications of TSL 1402, the applicable region in the amplitude-period plane is depicted.

Because of the chirped form of the homodyne signal, the spectrum of the signal has many higher harmonics of the vibration frequency [12]. The analog bandwidth of the instrument should pass Carson's bandwidth rule in order to transmit the intensity signal to an electrical one adequately. For TSL1402 with 8 MHz of operation, the analog bandwidth is not a constraining parameter.

In summary, in this Letter, we presented a new, simple, and low-cost direction-resolved homodyne LDV method. A linear array detector is used for recording successive 1D profiles of the time–evolved interference fringes. The successive 1D frames create a 2D STI. The produced STI is used for the vibration characterizing. We verified the method by vibrometry of a loudspeaker and used it for a vibration study of a thin-disk laser. In the presented method, the use of an array detector in the detection system simplifies the fringe chasing procedure and optical setup. In addition, by introducing the concept of a STI, the vibration waveform is directly determined without using the time-consuming SPS algorithm.

REFERENCES

1. R. Paschotta, R. T. Harald, and U. Keller, *Solid-State Lasers and Applications*, A. Sennaroglu, ed. (CRC Press, 2007), p. 473.
2. T. Nubbemeyer, M. Kaumanns, M. Ueffing, M. Gorjan, A. Alismail, H. Fattahi, J. Brons, O. Pronin, H. G. Barros, Z. Major, T. Metzger, D. Sutter, and F. Krausz, Opt. Lett. **42**, 1381 (2017).
3. T. Ryba, S. Zaske, S. S. Schad, and A. Killi, Proc. SPIE **10896**, 108960W (2019).
4. H. E. Albrecht, M. Borys, N. Damaschke, and C. Tropea, *Laser Doppler and Phase Doppler Measurement Techniques* (Springer, 2002).
5. R. J. Dewhurst and Q. Shan, Meas. Sci. Technol. **10**, R139 (1999).
6. A. C. Lewin, A. D. Kersey, and D. A. Jackson, J. Phys. E: Sci. Instrum. **18**, 604 (1985).
7. F. J. Eberhardt and F. A. Andrews, J. Acoust. Soc. Am. **48**, 603 (1970).
8. J. Czarske, Opt. Laser Technol. **33**, 553 (2001).
9. D. Jackson, A. Kersey, M. Corke, and J. Jones, Electron. Lett. **18**, 1081 (1982).
10. D. O. Hogenboom and C. A. DiMarzio, Appl. Opt. **37**, 2569 (1998).
11. J. Zhu, P. Hu, and J. Tan, Appl. Opt. **54**, 10196 (2015).
12. M. H. Daemi and S. Rasouli, Opt. Laser Technol. **103**, 387 (2018).
13. M. Saravani, A. Jafarnia, and M. Azizi, Opt. Laser Technol. **44**, 756 (2012).
14. M. Dashti and S. Rasouli, J. Opt. **14**, 095704 (2012).